Biogeosciences Discuss., 10, 18687–18722, 2013
www.biogeosciences-discuss.net/10/18687/2013/
doi:10.5194/bgd-10-18687-2013

Biogeosciences Discussions
Open Access

Pumping methane out of aquatic sediments – forcing mechanisms that affect the temporal dynamics of ebullition

A. Maeck[1], **H. Hofmann**[2], **and A. Lorke**[1]

[1]University of Koblenz-Landau, Institute for Environmental Sciences, Fortstr. 7, 76829 Landau, Germany
[2]University of Konstanz, Limnological Institute, Mainaustr. 252, 78464 Konstanz, Germany

Received: 4 September 2013 – Accepted: 22 October 2013 – Published: 28 November 2013

Correspondence to: A. Maeck (maeck@uni-landau.de)

Published by Copernicus Publications on behalf of the European Geosciences Union.

Abstract

Freshwater systems contribute significantly to the global atmospheric methane budget. A large fraction of the methane emitted from freshwaters is transported via ebullition. However, due to its strong variability in space and time, accurate measurements of ebullition rates are difficult; hence, the uncertainty of its contribution to global budgets is large. Here, we analyze measurements made by continuously recording automated bubble traps in an impounded river in central Europe and investigate the mechanisms affecting the temporal dynamics of bubble release from cohesive sediments. Our results show that the main mechanisms for bubble release were pressure changes, originating from the passage of ship-lock induced surges and ship-passages. The response to physical forcing was strongly affected by previous outgassing. Ebullition rates varied strongly over all relevant timescales from minutes to days; therefore, representative ebullition estimates could only be inferred with continuous sampling over long periods. Since ebullition was found to be episodic, short sampling intervals of a few days or weeks will likely underestimate ebullition rates, which may result in an uncertainty of over 50 % in current global freshwater emission estimates.

1 Introduction

Methane (CH_4) is regarded as the second most important anthropogenic greenhouse gas with global emissions between 500 and 600 $Tg\,yr^{-1}$ (Forster et al., 2007). The contribution of freshwater systems is estimated to be around 103 $Tg\,CH_4\,yr^{-1}$, of which over 53 % are emitted via gas bubbles (Bastviken et al., 2011).

Gas bubbles released from anoxic freshwater sediments often consist of a large proportion of CH_4 (Baulch et al., 2011). In these sediments where alternative electron acceptors, e.g. nitrate or sulfate, are lacking or depleted and degradable organic carbon (C_{org}) is available, CH_4 is produced by organisms of the domain archaea. The rate of production depends on the amount and quality of C_{org} and temperature (Duc et al.,

BGD
10, 18687–18722, 2013

2010; Liikanen and Martikainen, 2003; Segers, 1998; Sobek et al., 2012). Produced CH_4 can dissolve into the porewater and thus, continuous production in combination with low efflux rates can lead to high concentrations of CH_4 within the porewater (Maeck et al., 2013). If the partial pressure of all dissolved gases (mainly CH_4 and N_2) in the porewater exceeds the ambient pressure and the surface tension of water, free gas is formed. Due to ongoing production of CH_4, bubbles within the sediments grow and form fractures or disc shaped cavities (Boudreau et al., 2005; Johnson et al., 2002).

The transport mode of CH_4 from the sediments to the atmosphere has important implications. Transport via diffusion is relatively slow and methane oxidizing bacteria can oxidize a large proportion of the produced CH_4 (Segers, 1998). Surface waves are known to increase the near-bottom current velocities and to cause sediment resuspension in the shallow littoral, which triggers and accelerates the flux of methane across the sediment–water interface (Hofmann et al., 2010). Further, evading free gas in form of rising bubbles is transported too fast for microbial oxidation at the sediment–water interface. However, if bubbles are slowly transported through the upper layer of sediment, where O_2, NO_3^- or SO_4^{2-} is present, a fraction of the free CH_4 gas can be oxidized, which was shown by carbon isotopic signatures (Venkiteswaran et al., 2013). In terms of atmospheric emissions, physical and chemical parameters like the water depth, bubble size and the concentration of CH_4 in the ambient water determine what fraction of the initially released CH_4 reaches the atmosphere (Leifer and Patro, 2002; McGinnis et al., 2006). While the fate of rising CH_4 bubbles in the water column is well understood (Leifer and Patro, 2002; McGinnis et al., 2006), studies investigating the mechanisms responsible for the temporal and spatial dynamics of bubble release are rare. The spatial variability of ebullition in impounded rivers was recently shown to correlate strongly with spatial patterns of sedimentation (Maeck et al., 2013). In a large reservoir, DelSontro et al. (2011) found higher ebullitive fluxes in river delta bays compared to non-river bays which may also point towards sedimentation as the main cause for the spatial distribution of ebullition. Within this work, we focus on the temporal variability of ebullition at greater detail and investigate the underlying processes.

BGD
10, 18687–18722, 2013

Most studies suggest that ebullition occurs episodically (Coulthard et al., 2009; Goodrich et al., 2011; Varadharajan and Hemond, 2012). The episodic pattern may be related to a complex interplay between bubble buoyancy and sediment mechanics. Numerical modeling suggests that bubble rise within the sediment is driven by dilating conduits or rise tracts ("transport pipes") which facilitate gas transport due to their higher flow conductance (Scandella et al., 2011). The mechanism dilating the conduits and therefore controlling the temporal pattern of bubble release is assumed to be hydrostatic pressure (Scandella et al., 2011). Another study showed that shear-stress at the sediment–water interface is correlated with ebullition rates (Joyce and Jewell, 2003). The origin of hydrostatic pressure or shear-stress changes can be various physical phenomena, e.g. waves or water level changes, which are further denoted as forcing mechanisms. Studies showed that forcing mechanisms affecting ebullition rates can be air pressure changes, tides, wind or water level changes and that the temporal variability is high (Chanton et al., 1989; Joyce and Jewell, 2003; Varadharajan and Hemond, 2012).

The timescales at which forcing mechanisms trigger ebullition are variable, e.g. ship-induced surface waves act as a single event on timescales of seconds to minutes, while air pressure or water level changes can vary significantly at scales of days to weeks. And since ebullition rates are directly affected by the temporal dynamics of forcing mechanisms, we hypothesize that both are strongly correlated.

Within this study, we used automatic bubble traps (ABTs) to measure ebullition rates with a high temporal resolution continuously over five months in an impounded river in central Europe. The data are analyzed in combination with timeseries of hydrostatic and air pressure (as well as other parameters) to investigate the relationship between forcing mechanisms and gas release at greater detail. The scope of this study is (1) to quantify the temporal variability of ebullition rates in an impounded river, (2) to estimate the relevant time scales of variability, and (3) to identify the corresponding forcing mechanisms. Furthermore, we will use these results to review the methodologies and

BGD
10, 18687–18722, 2013

potential uncertainties associated with limited sampling periods of ebullition measurements described in the literature.

2 Material and methods

2.1 Study site

Flowing along 246 km through France and south-west Germany, the River Saar discharges a watershed of 7.363 km^2 in central Europe. The mean discharge at the gauging station Fremersdorf (km 48) is 75 $m^3 s^{-1}$. During the period January 2010 to February 2013, the discharge ranged often between 20 and 40 $m^{-3} s^{-1}$ ($\sim$ 60 % of all days) but also peaks up to 675 $m^{-3} s^{-1}$ occurred. The German part of the river (the lower 96 km) was impounded between 1976 and 2000 for navigation purposes. Therefore the river bed was channelized over long distances and six dams with ship-locks and hydropower plants were built.

The damming of the river led to increased water depths (up to 11 m), prolonged water residence times (Schöl, 2006), and strong sedimentation upstream of the dams where the flow velocity is reduced (Maeck et al., 2013). To maintain cargo shipping, the riverbed is dredged on demand to ensure a minimum shipping depth of 4 m within the shipping channel. However, sediment layers of up to 5 m thickness exist in zones outside of the shipping channel, e.g. at the inner bending of river meanders. A longitudinal study along the entire River Saar showed that most of the methane emissions (> 90 %) originate from the zones of high sedimentation that are located upstream of the dams (Maeck et al., 2013). These zones exhibit a more reservoir-like than riverine character with reduced flow velocities, thermal stratification during periods of high solar radiation, and higher average water depths (Becker et al., 2010).

For this study, we measured ebullition and pressure at three sites approximately 1 to 2 km upstream of Serrig Dam (Fig. 1). This river stretch is characterized by intensive

BGD
10, 18687–18722, 2013

sediment accumulation (1 to 5 m within the period of 1993 and 2010, Fig. 1b) and strong methane ebullition (Maeck et al., 2013).

The water level in the Serrig impoundment is regulated by Serrig Dam, but water im- or export from ship-lock chambers induces strong short-term discharge changes, which propagate as surges (Maeck and Lorke, 2013). Surges are gravity waves, either shaped as a solitary wave crest (positive surge) or trough (negative surge), which propagate along the entire basin, are reflected at the next dam and propagate backwards (USACE, 1949). Superposition of multiple surges led to water level fluctuations of up to ∼ 30 cm, which is comparable to long-term reservoir storage changes (Maeck and Lorke 2013). Associated with water level changes during the passage of surges are changes in the mean flow velocity, which can create flow reversals (Maeck and Lorke, 2013).

2.2 Measurement of ebullition rates

Ebullition was measured continuously using three ABTs at sites with a net sediment accumulation rate of 0.29, 0.07 and 0.1 m yr^{-1}, respectively (1993–2010; Fig. 1b, Maeck et al., 2013). An ABT consists of an inverted polypropylene funnel with a diameter of 1 m, a cylindrical gas capture container (diameter 23 or 29 mm), a differential pressure sensor (PD-9/0.1 bar FS, Keller AG) and a custom-made electronic unit (data logger and regulation device for venting the gas capture container, Fig. 2b). The entire ABT was deployed submerged so that rising gas bubbles within the water column were collected by the funnel and the gas accumulates in the cylindrical container. The water level within this container was monitored at an interval of 5 s using the differential pressure between inside the container and outside. The amount of gas was calculated using the ideal gas law

$$n = \frac{p_i \cdot (\pi \cdot r^2 \cdot H)}{R \cdot T} \quad (1)$$

BGD
10, 18687–18722, 2013

where n denotes the number of moles [mol], p_i the partial pressure of CH_4 [Pa], r the radius of the cylindrical gas container [m], H the measured fill height [m], R the universal gas constant [$m^3\,Pa\,K^{-1}\,mol^{-1}$] and T the temperature [K]. Temperature measurements were performed using an RBR TR-1060 sensor with an accuracy of ±0.008 °C attached to the ABTs. The partial pressure was calculated as the product of absolute pressure (10^5 Pa or 1 bar) and the mean mole fraction of CH_4 in the gas bubble (0.80, see results section).

By using the number of moles of CH_4 (n), the base area of the funnel A [m], and the timestamps of the datalogger (t_{i+1} and t_i) [d], the ebullition rate E [$mol\,m^{-2}\,d^{-1}$] was estimated as

$$E = \frac{n}{A \cdot (t_{i+1} - t_i)} \quad (2)$$

Every four weeks, the system was recovered for cleaning, data download, calibration and battery replacement. For calibration of the differential pressure sensor the capture container of each ABT was submersed in a glass cylinder and air was injected manually to achieve a specific fillheight measured visually with an attached scale bar. An average differential pressure sensor reading was recorded for five different fillheights and linear regression analysis was used to determine the corresponding calibration coefficients. The goodness-of-fit R^2-value was always > 0.98. A temperature correction was applied electronically within the electronic unit.

The gas capturing container was automatically emptied as soon as the captured gas reaches the storage capacity. Therefore, the electronic unit opens a solenoid valve which vents the system and a new measurement cycle starts.

The nominal accuracy of the differential pressure sensor given by the manufacturer is 50 Pa which corresponds to a water level of approximately 0.5 cm. Since absolute accuracy increases linearly with the difference of water level within the container at two points in time, the accuracy increases with ebullitive rate. However, each system venting decreases the accuracy since two additional measurements are required for each venting; one at the maximum fill level and one base value, when the system is emptied

BGD
10, 18687–18722, 2013

completely (Fig. 2). Therefore, the accuracy is non-linear but above volume measurements of 410 and 640 mL gas with the 23 and 29 mm container diameters (13.5 and 21.3 mmol CH_4 at 20 °C, 1 bar and assuming 80 % CH_4 content in the captured gas, repectively) is always below 10 %. Thus, high ebullition rates can be quantified with the ABT over long periods with an error of less than 10 %.

2.3 Pressure measurements

Hourly mean air pressure data were obtained from the German Weather Service (station Trier-Petrisberg 49.7492° N, 6.6592° E), located approximately 20 km north of the sampling sites.

We deployed a RBR-2050 (RBR Ltd., Canada) pressure and temperature sensor (LR-PS) on the riverbed close to the automated bubble trap ABT-1 (Fig. 1b) during the study period from 16 October 2012 to 6 March 2013. Data was recorded at an interval of 5 s. The accuracy of the pressure sensor is 0.25 mbar at a resolution of 0.05 mbar, while the accuracy of the temperature sensor is ±0.008 °C.

To characterize the surface wave field, a custom-made high-resolution pressure sensor (HR-PS) (Hofmann et al., 2008) was deployed in the vicinity of ABT-1 at a height of ∼ 1 m above the riverbed in ∼ 1.8 m water depth (Fig. 1b). Data was recorded at a frequency of 16 Hz.

2.4 Concentration of CH_4 within the bubbles

To determine the concentration of CH_4 within gas bubbles, an anchor weight of > 10 kg was used to disturb the sediment surface and release bubbles in a distance of approximately 5 to 8 m from the ABTs. They were caught immediately in the first 1.5 m of their rise with an inverted funnel (diameter 0.6 m) equipped with a 1.5 L gas container. The gas was transferred with a syringe to triplicate brine-filled (saturated NaCl-solution) 20 mL headspace vials sealed with a butyl-rubber stopper. An injected needle allowed brine to flow out while the gas was transferred from the syringe into the vial. Approx-

BGD
10, 18687–18722, 2013

imately 5 mL of brine remained in the vials as a diffusion barrier to minimize leakage when the vials were stored upside down. CH_4-concentration in the headspace was measured in the lab using gas chromatography (Varian, CP-3800, flame-ionization detector).

2.5 Analysis

2.5.1 Estimating the error of the monthly mean ebullition rate by subsampling

Our dataset consists of continuous (5 s interval) measurements of ebullition rates over five months. Subsets of 1 to 720 consecutive hours were drawn from the total dataset. The mean ebullition rate of the subset $\overline{E_{\text{subset}}}$ was compared with the mean ebullition rate of the surrounding 30 days $\overline{E_{30\,\text{days}}}$ including the subset (e.g. for a subset of 24 h, the 14.5 days before, the 24 h subset and the 14.5 days after the subset were used), where D denotes the deviation of the subset from the monthly mean in %

$$D = \frac{\overline{E_{\text{subset}}}}{\overline{E_{30\,\text{days}}}} \cdot 100\,\% \tag{3}$$

The subsets were shifted through the entire dataset so that the results of many subset deviations were used to calculate the 10-, 50- and 90-percentile deviation from the 30-days mean ebullition rate.

2.5.2 Frequency spectrum

To determine the relevant timescales of pressure variability and ebullition we estimated power spectral density using Welch's method with a Hamming-window and 50 % overlap (Emery and Thomson, 2001). In the ebullition dataset, the instantaneous ebullition rate with a sampling interval of 5 s was used after exclusion of outliers (> 1000 times the average ebullition rate). The window size for the ebullition rate spectrum was 2^{14}

BGD
10, 18687–18722, 2013

measurements for periods < 24 h and 2^{20} for periods > 24 h to combine both spectra to a composite spectrum. For the LR-PS and HR-PS data, 2^{19} samples were used.

2.5.3 Characterizing low and high pressure variability periods

The contributions of surface waves and surges to the total variability of hydrostatic pressure were discriminated using a high-pass filter (5th order Butterworth) with a cut-off frequency corresponding to a 6 h period. By using a running-standard deviation (RSTD, window size 30 min) on the high-frequency pressure signal, periods of high and low variability were identified. The pressure data were divided in 1 h windows and the mean of the RSTD of the window was compared to the mean RSTD of the entire timeseries. Windows with an average RSTD below the RSTD of the entire timeseries were categorized as "low variability periods" while periods with a RSTD above the mean RSTD were designated as "high variability periods".

2.5.4 Determining trigger mechanisms for ebullition

Since the actual hourly emission rate varies strongly and the volume of gas released is not a linear function of the forcing mechanism, we used a logistic regression analysis to analyze the relative importance of different forcing mechanisms. Hourly mean ebullition rates were assigned to a logical number of 1 if ebullition rates were higher than the mean emission rate of the entire measurement period and 0 for lower values. As explanatory forcing mechanisms we considered the change in barometric pressure, low-frequency filtered (6 h cut-off period) hydrostatic pressure, hydrostatic pressure fluctuations determined as the standard deviation of the high-frequency filtered hydrostatic pressure, the total gas flux within the previous 24 h and discharge. All forcing mechanisms were determined for the same period as the ebullition rate, except for the total gas flux of the previous 24 h.

All partial regression coefficients were normalized to represent the relative contribution of each factor to the total variability of the ebullition rate. Therefore, the output

BGD
10, 18687–18722, 2013

metric partial regression coefficients were multiplied by the standard deviation of the explanatory variable and divided by the standard deviation of the ebullition rate.

3 Results

3.1 Physical environment

During the study period from 16 October 2012 to 6 March 2013, the discharge ranged from 18.5 to 405 $m^3 s^{-1}$ (gauging station Fremersdorf) with an average of 109 $m^3 s^{-1}$ and a median of 63 $m^3 s^{-1}$. Over 50 % of all days, the discharge was below 65 $m^3 s^{-1}$. Three major flood peaks occurred from 2 to 13 November, 14 December to 8 January, and 28 January to 14 February (Fig. 3). Water temperature ranged between 2.8 °C and 13.5 °C (Fig. 3). From 16 to 27 October, diurnal thermal stratification occurred. The water column was well mixed during the rest of the study period.

The total pressure at the sediment surface is the sum of atmospheric pressure at the water surface and gravitational pressure imposed by the water column, which is controlled by the water level. Both parts contributed with similar magnitudes to the observed variability of total pressure at the sediment surface (76 % of the total variation is contributed by hydrostatic and 24 % by atmospheric pressure changes), but show distinct differences in the spectral distribution of variance (Fig. 4). While both air pressure and water level varied on timescales of days to weeks, the hydrostatic pressure also showed strong variability on the timescale of minutes to hours (Fig. 3), which is in most cases the result of ship-lock induced surges (Peaks in Fig. 4 at 15 min, 32 min and 65 min) (Maeck and Lorke, 2013). Since the water level is regulated by Serrig Dam, maximum changes in water level, even during high-discharge periods, were below 0.74 m while the standard deviation of the water level was 0.07 m (Fig. 3).

Analysis of the high-pass filtered hydrostatic pressure signal of the LR-PS allowed distinguishing periods with high and low pressure variability. The high variability periods were characterized by intensive ship-locking activity that induced multiple surges

BGD
10, 18687–18722, 2013

(Maeck and Lorke, 2013) and corresponding passages of ships were observed. The passage of a surge is characterized by a defined wave crest or trough over a period of ∼ 12 min while the passage of a ship often showed a strong (up to 30 cm of water level) but short (< 1 min) decrease in pressure in the LR-PS signal. In the HR-PS measurements, ship-waves could be discriminated from wind-induced surface waves by their short duration and due to their higher maximum wave amplitude. We chose a threshold of 2 cm for separation. Ship-waves showed on average a maximum wave height of 4.2 cm; however, they often reached maximum wave heights between 10 and 20 cm.

3.2 Characterization of ebullition

Deliberately released gas bubbles had CH_4 volume concentrations between 48.6 % and 92.1 % with a mean of 80.5 %. For the conversion of the volume measurements with the ABTs to the ebullition rate, a concentration of 80 % CH_4 was used (Table 1).

We observed high variability in the ebullitive flux at all temporal scales ranging from minutes to days (Fig. 5). The daily ebullition rate ranged from 0 up to 240, 48 and 147 mmol CH_4 m^{-2} d^{-1} for ABT-1, ABT-2 and ABT-3, respectively. The mean daily ebullition rate for the entire sampling period was 32±37, 7±8 and 15±23 mmol CH_4 m^{-2} d^{-1}, at ABT-1, ABT-2 and ABT-3 respectively (mean ±1 standard deviation). From October to the end of January, the mean monthly ebullition rate showed no trend, while in February, the ebullition rate increased strongly for ABT-1 and ABT-3.

Most of the variability of the ebullition rate occurred on short timescales below one day (Fig. 4), e.g. the 5 min ebullition rate varied much stronger compared to 1 h or 1 d ebullition rate (Fig. 5). The frequency distribution of spectral variance (Fig. 4) shows that most variability is associated with time scales between 1 min and 2 h. But also distinct peaks at higher frequencies with corresponding time periods of < 1 min were observed. These high-frequency spectral peaks, however, are potentially measurement artefacts caused, for example by surface wave-induced oscillations of the ABT mooring as well as by the discrete nature of ebullition. Also longer-term variability (e.g. day to

BGD
10, 18687–18722, 2013

day changes of ebullition rates) exceeding one order of magnitude occurred frequently. Therefore, a representative estimate of the monthly mean ebullition rate can only be determined after long measurement periods. The inter-percentile range between the 10 and 90-percentile of the subset mean ebullition rate was high for sampling durations of several hours and decreased with increasing measurement length (Fig. 6). The chance to estimate the 30-days mean ebullition rate with a precision of ±50 % is 80 % after measurements of consecutive 303, 375 or 280 h for ABT-1, ABT-2 and ABT-3 respectively.

Ebullition occurred episodically, often in bursts of several bubbles entering the bubble trap indicated by the observation that the volume measured every 5 s often exceeded the volume of a typical bubble having a 5 mm diameter and a volume of ∼ 0.5 mL (McGinnis et al., 2006). Not all but many bursts were synchronized between all three ABTs (Fig. 7). The cross-correlation between ABTs shows a distinct maximum at zero lag, which indicates that a major portion of ebullition events are synchronized. Secondary small peaks were observed at ±1 h time lag, which corresponds to the reoccurrence of ship-lock induced surges after propagation along the entire impoundment, reflection and backward propagation (Maeck and Lorke, 2013).

3.3 Mechanisms triggering ebullition

Analysis of all synchronized 5 min ebullition rates, where all ABTs measured values exceeding 56 mmol CH_4 m^{-2} d^{-1} (corresponding to ∼ 1 g CH_4 m^{-2} d^{-1}), shows that 59.4 % of all investigated ebullition rates occurred during the passage of a negative ship-lock induced surge (wave trough), 26.4 % during the passage of a ship, 5.7 % during periods of sinking water level and 7.5 % during times where no pressure change was observed. Only one of the investigated ebullition events (0.9 %) was observed during the passage of a positive surge. The detailed temporal dynamics of ebullition rates in relation to the major forcing mechanisms are exemplified in Fig. 8. The physical forcing of bubble release by surges and ship passages was the major regulator for the timing of ebullition.

BGD
10, 18687–18722, 2013

However, we also observed examples where no response of ebullition followed these forcing events.

The multiple logistic regression analysis revealed that ebullition within the previous 24 h and high frequency pressure fluctuations are the most important parameters for explaining the observed variability of ebullition rates (Table 2). Both parameters decreased the ebullition rate indicated by a negative regression coefficient. The hydrostatic pressure varied strongly during 46 % of the entire sampling period due to shiplock and ship activity (Maeck and Lorke, 2013), but contributed 61 %, 72 % and 66 % to the total gas flux variability at ABT-1, ABT-2 and ABT-3 respectively. Mean emission rates during high pressure variability periods (44, 12 and 21 mmol CH_4 m^{-2} d^{-1}), mostly occurring at daytime due to intensive ship activity (Maeck and Lorke 2013), were higher compared to emission rates during low pressure variability periods (22, 4 and 8 mmol CH_4 m^{-2} d^{-1} for ABT-1, ABT-2 and ABT-3, respectively).

4 Discussion

4.1 Variability and magnitude of ebullitive emissions

All sampling sites of this study are characterized by high sediment accumulation, which promotes high production rates of CH_4 (Maeck et al., 2013). The trend that ebullition rate positively correlates with sediment accumulation rates observed by Maeck et al. (2013) holds true also for the long-term measurements presented here. ABT-1 located over a site with the highest sediment accumulation rate (0.29 m yr^{-1}, Fig. 1, determined following Maeck et al., 2013) showed the highest mean ebullition rate, followed by ABT-3 and ABT-2 with sediment accumulation rates of 0.1 and 0.07 m yr^{-1}, respectively. Therefore, the production rate per square meter likely differs between the three sites. We observed that with increasing production rate, estimated by using the sedimentation rate as a proxy, the variability in the daily ebullition rate increased, which may be the effect of frequent forcing in combination with the production rate (Fig. 9).

BGD
10, 18687–18722, 2013

The magnitude of CH_4 ebullition rates measured in the present study are lower compared to the results of Maeck et al. (2013), which may be the result of differing sediment temperature. While the data presented here were measured during the winter when temperatures were low, the study by Maeck et al. (2013) was performed in September when water temperatures were higher. However, these current results are higher than total CH_4 emission rates reported for temperate lakes, rivers or reservoirs and comparable to emissions of tropical ($< 25^{\circ}$ latitude) reservoirs (Bastviken et al., 2011; Varadharajan and Hemond, 2012) as was also observed in a Swiss hydropower reservoir (DelSontro et al., 2010). The temporal variability of ebullition rates was extremely high, as observed by Varadharajan and Hemond (2012); hence, for reliable measurements of ebullitive emissions the temporal variability must be considered in the planning stages of future studies.

Our results show clearly that ebullition is episodic, occurring in bursts consisting of many bubbles. The reason for this can be two-fold. On the one hand, external forcing (e.g. pressure reduction) can increase the volume of all bubbles within the sediment, from which a portion then has a buoyancy exceeding the strength of the surrounding sediment and start to rise (Boudreau et al., 2005). On the other hand, as soon as the first bubbles rise, they form conduits or rise tracks that make it easier for other bubbles to follow (Boudreau et al., 2005; Scandella et al., 2011). Besides external forcing, bubbles can also be released by ongoing CH_4 production and continuous bubble growth and rise. This mechanism would lead to unsynchronized ebullition rates between sites and, when averaged over longer timescales, to constant flux rates that will then respond to changes in CH_4 productivity, e.g. due to temperature changes. The results of this study show, however, that mechanical forcing dominates the temporal pattern of ebullition, not continuous CH_4 production.

During our study period, temperatures in the water column were low and ranged mostly between 3 and 8 °C. However, since CH_4 production occurs mainly within the sediments at our sampling sites (Maeck et al., 2013), the temperature within the sediment is the effective temperature regulating biogeochemical reaction kinetics and

BGD
10, 18687–18722, 2013

therefore CH_4 production. Sediment temperature itself is affected by heat exchange with the overlying water column, with the groundwater, and to a lesser extent by microbial heat production associated with the degradation of organic matter (Fang and Stefan, 1996, 1998). Only the top layer of the sediment is strongly affected by heat exchange with the overlying water column and therefore subject to pronounced temperature variations, while the temperature variability decreases with increasing depth (Fang and Stefan, 1998). Since water temperatures were low, we assume that during our study period the production zone of methane was mainly within deeper sediment layers, where the effective temperature for methanogenesis changed only slowly compared to the timescale of forcing mechanisms. No direct relationship between water temperature and ebullition rate was observed, indicating that the temperature within the sediment responds only slowly to water temperature changes. The high degree of synchronization (Fig. 7) and the observation that most of the gas was released during high-variability periods of hydrostatic pressure reveal the importance of the forcing regime for the temporal pattern of bubble release. In the case of the River Saar, physical forcing mechanisms control the temporal dynamics of ebullition on short timescales.

4.2 Forcing mechanisms

The major trigger mechanisms for ebullition were changes in hydrostatic pressure, primarily due to ship-lock induced surges and ship-passages. However, the magnitude of ebullition was also affected by the previous history of gas venting, i.e. in the last 24 h. The negative relationship we found between ebullition rate and gas flux in the last 24 h indicates that the amount of gas previously released impacts current ebullition rates. This would imply that a forcing such as a surge or ship passage could cause no bubble release at certain times. The majority of large ebullition events matched clearly with pressure reductions due to ship-locking and ship passages as reported for other pressure changing mechanisms (Chanton et al., 1989; Joyce and Jewell, 2003; Varadharajan and Hemond, 2012). Therefore we expected a positive regression coefficient for high-frequency pressure fluctuations. However, the coefficient was negative, which

BGD
10, 18687–18722, 2013

points towards an interference with previous gas release since pressure fluctuations are often present for several hours in response to intensive ship-lock and shipping activity.

The passage of ships associated with different types of surface waves affected ebullition (Fig. 8c). However, ships can cause very different pressure changes and wave characteristics at the sampling site depending on the type of ship, its speed, the actual pathway of the ship-track and the direction of the slipstream (Hofmann et al., 2008). Therefore, the passage of ships can but will not always trigger ebullition. The example of Fig. 8 shows that several ship-passages had a strong effect on ebullition at ABT-1, but nearly no effect for the other two ABTs. This can result from the location of the ABTs and the morphology of the different sites. While ships passed closer to ABT-1, ABT-2 and ABT-3 were further away from the main shipping channel and closer to the shore. Propagating diverging ship-waves attenuate with travel length (Kundu and Cohen, 2008), but since the ABT-2 and ABT-3 were closer than 80 m to the bypassing ships, the attenuation is of minor importance; therefore, the ship-waves must have been also present at the locations of ABT-2 and ABT-3. The missing gas release at ABT-2 and ABT-3 indicates that at ABT-1 the ebullition was not triggered by diverging surface waves but rather by other processes in the vicinity of the ship, e.g. draft-induced pressure changes. However, we observed visually during our field campaigns that gas bubbles were released massively following the passage of large ship-waves, but only in the more shallow areas (< 2 m water depth). Since the pressure signal caused by surface waves decreases with increasing depth and decreasing wave length (Kundu and Cohen, 2008), short waves, e.g. wind-induced or diverging ship waves, change the pressure at the sediment surface only in shallow regions while long waves, e.g. surges affect also the pressure in deeper areas.

Negative surges with a decrease in pressure showed stronger effects on ebullition compared to positive surges, which increase the pressure temporarily. Since the passage of both surges is associated with similar changes in current velocity (Maeck and Lorke, 2013), the effect of shear-stress and pressure change on ebullition rates can be

BGD
10, 18687–18722, 2013

discriminated. Negative surges reduce the pressure while positive surges increase the pressure. Significantly more large ebullition events co-occurred with negative surges, which indicates that the effect of pressure changes were stronger compared to shear-stress (Fig. 8b, results section).

Sinking water level can also be a driver for bubble release (Fig. 8a), but in the case of the River Saar this effect was of minor importance. Temporal changes in storage height may be much more important for systems with strong changes in water level, e.g. caused by hydropower peaking (Zohary and Ostrovsky, 2011).

The timescale of the relevant forcing mechanisms is in the order of seconds (ship-waves), minutes (surges) and hours (sinking water level). Often, multiple occurrences of the individual mechanisms, e.g. during periods of intensive ship-traffic, led to pronounced pressure fluctuations which caused gas venting from the sediments. We observed periods over which the forcing mechanisms are constantly active (periods of high-variability in hydrostatic pressure), e.g. during the day, and periods of negligible forcing and lower ebullition rates (i.e. during the night). Since CH_4 production is continuously ongoing, forcing decouples production and gas release. The sediment acts therefore as a storage system for free gas, which further emphasizes the importance of forcing mechanisms for the temporal dynamics of gas release.

5 Implications

5.1 Timescale of forcing in other aquatic systems

The temporal dynamics of forcing mechanisms can be expected to differ among different aquatic systems. In lakes for example, water level changes are often caused by changes in the inflow of rivers on a timescale of days to weeks (Hofmann et al., 2008; Jöhnk et al., 2004; Wilcox et al., 2007). In large lakes, having sufficient fetch length for wind energy input, seiches and propagating surface waves can generate short-term pressure fluctuations (Hamblin and Hollan, 1978). In lakes with limited fetch

BGD
10, 18687–18722, 2013

length, atmospheric pressure changes have been demonstrated to control ebullition rates (Varadharajan and Hemond, 2012). In reservoirs, the inflow of water and the operation of dams are important, since pressure is predominantly controlled by the water level. In these systems, water level drawdown can trigger ebullition, but also wind speed may affect gas venting (Joyce and Jewell, 2003). In tidal systems, ebullition rates were shown to be controlled by the tidal rise and fall of the water level (Boles et al., 2001). In general, many inland waters are exposed to periodically occurring forcing mechanisms with associated periods similar to those observed at the Saar.

The temporal pattern of ebullition from cohesive sediments is governed by two major factors: the production rate of CH_4 (here estimated by using the sedimentation rate as a proxy) and the timescale of forcing of sufficient magnitude to release bubbles (Fig. 9) ~~to release bubbles.~~ Under low production rates and short-term (high-frequency) forcing conditions, the ebullition rate may be relatively constant on the timescale of several days, since all bubbles exceeding a specific size are released immediately by forcing (Fig. 9c). Short-term forcing in combination with high CH_4 production leads to the pattern observed within this study (Fig. 9a) characterized by strongly variable ebullition rates on short timescales, but relatively constant fluxes after averaging over several days. Low production sites with long-term (low-frequency) forcing mechanisms will release bubbles mainly during times of significant forcing, e.g. during water level reduction (Fig. 9d) as observed by Varadharajan et al. (2012). Highly productive systems exposed to long-term forcing may release bubbles continuously following at the rate of CH_4 production (Fig. 9b) (Maeck et al. data from the impoundment Krotzenburg of the River Main, measured with the same instrumentation and analyzed with the same methods as in this study). Therefore, the ebullition rate may vary only little on timescales of days, but enhanced ebullition can occur during forcing periods, e.g. during periods of decreasing atmospheric pressure. To verify this conceptual framework, which provides a useful a-priori estimate of the temporal variability of CH_4 ebullition in aquatic systems, more high-resolution long-term ebullition data of different sites in combination with measurement of forcing parameters are necessary.

BGD
10, 18687–18722, 2013

5.2 Implications for sampling and global estimates

The recently developed guidelines for measuring greenhouse gas emissions from reservoirs (UNESCO/IHA, 2011) recommend to perform ebullition measurements over a period of at least 24 h. In the River Saar, we observed a daily pattern with higher fluxes during the day when ship-locking and ship-traffic induces water level fluctuations. During the night when ship traffic decreased, the water level fluctuations decreased and the ebullition rate was lower. Therefore, it is necessary to sample day and night. However, since forcing can be of varying magnitude, the daily ebullition rate varied strongly and therefore, in the River Saar, ebullition measurements over 24 h are not representative for longer periods (Fig. 6).

To determine the period of representative measurement, the variability in the ebullition rate itself is not the most important factor but rather the temporal distance between episodes of strong gas release ("bubbling episodes"). For accurate extrapolation of short-term measurements to longer periods, it is necessary to measure over periods which cover the timescale of the bubbling episodes several times since there is variability between the episodes (Fig. 5) (Varadharajan and Hemond, 2012). A representative measurement period at the Saar has to cover more than 10 days (indicated by the median in Fig. 8). In aquatic systems with longer periods between bubbling episodes, representative sampling periods will be much longer.

Short measurement durations are likely to underestimate the ebullition rate significantly since the median flux in Fig. 6 is mostly smaller than 50 % of its monthly mean value. On the contrary, if measurements are mainly performed during day time, ebullition rates are likely to be overestimated because some forcing mechanisms, like wind or ship-induced forcing, are more likely to occur during the day. If measurements are performed during randomly chosen periods of 24 h or shorter (< 24 h), the chance to underestimate ebullition rates by over 50 % is large (average median of 54 % underestimation at 24 h in Fig. 6).

BGD
10, 18687–18722, 2013

These findings have potential implications for current estimates of global freshwater emissions of CH_4. Current guidelines and also technical limitations allow most studies to measure ebullition rates only over short time periods (e.g. over 24 h or less). These measurements form the basis for bottom-up approaches for estimating the global CH_4 emissions from freshwater systems, where ebullition is the predominant emission pathway and contributes ~ 53 % to total emissions (Bastviken et al., 2011). Based on our observations, that ebullition could potentially be underestimated by 50 %, global ebullitive emissions from freshwater systems could be up to 108 Tg CH_4 yr^{-1} (which increases the current estimate to 155 Tg CH_4 yr^{-1}; Bastviken et al., 2011). However, our observations are made in a heavily human-impacted system with high ebullition rates and thus not representative for all aquatic systems. To achieve more accurate emission estimates, we recommend to monitor ebullition over long sampling periods, and to take the temporal variability caused by system-specific forcing periods into account when planning and analyzing ebullition measurements in aquatic systems.

Acknowledgements. The authors would like to thank the Water and Shipping Agency Saarbrücken (WSV) for their great support during deployment of the ABTs and Helmut Fischer from the Federal Institute of Hydrology (BfG) for providing infrastructure and administrative support. Special thanks go to Florian Mäck who developed the electronic part and the software interface of the ABTs and to Sebastian Geissler, who constructed the housing and his support during the field campaigns. We would like to thank the team of Lothar Laake of the workshop of the University of Göttingen for manufacturing the housing and Dan McGinnis and Tonya DelSontro for sharing the mechanical construction of the ABTs. This study was financially supported by the German Research Foundation (grant LO 1150/5-1).

References

Bastviken, D., Tranvik, L. J., Downing, J. A., Crill, P. M., and Enrich-Prast, A.: Freshwater methane emissions offset the continental carbon sink, Science, 331, 50, doi:10.1126/science.1196808, 2011.

BGD
10, 18687–18722, 2013

Baulch, H. M., Dillon, P. J., Maranger, R., and Schiff, S. L.: Diffusive and ebullitive transport of methane and nitrous oxide from streams: are bubble-mediated fluxes important?, J. Geophys. Res.-Biogeo., 116, doi:10.1029/2011JG001656, 2011.

Becker, A., Kirchesch, V., Baumert, H. Z., Fischer, H., and Schöl, A.: Modelling the effects of thermal stratification on the oxygen budget of an impounded river, River Res. Appl., 26, 572–588, doi:10.1002/rra.1260, 2010.

Boles, J., Clark, J., Leifer, I., and Washburn, L.: Temporal variation in natural methane seep rate due to tides, Coal Oil Point area, California, J. Geophys. Res.-Oceans, 106, 27077–27086, doi:10.1029/2000JC000774, 2001.

Boudreau, B. P., Algar, C., Johnson, B. D., Croudace, I., Reed, A., Furukawa, Y., Dorgan, K. M., Jumars, P. A., Grader, A. S., and Gardiner, B. S.: Bubble growth and rise in soft sediments, Geology, 33, 517–520, doi:10.1130/G21259.1, 2005.

Chanton, J. P., Martens, C. S., and Kelley, C. A.: Gas transport from methane-saturated, tidal freshwater and wetland sediments, Limnol. Oceanogr., 34, 807–819, 1989.

Coulthard, T., Baird, A., Ramirez, J., and Waddington, J.: Methane dynamics in peat: importance of shallow peats and a novel reduced-complexity approach for modeling ebullition, carbon cycling in Northern Peatlands, Geophys. Monogr. Ser, 184, 173–185, doi:10.1029/2008GM000811, 2009.

DelSontro, T., McGinnis, D. F., Sobek, S., Ostrovsky, I., and Wehrli, B.: Extreme methane emissions from a Swiss hydropower reservoir: contribution from bubbling sediments, Environ. Sci. Technol., 44, 2419–2425, doi:10.1021/es9031369, 2010.

DelSontro, T., Kunz, M. J., Kempter, T., Wüest, A., Wehrli, B., and Senn, D. B.: Spatial heterogeneity of methane ebullition in a large tropical reservoir, Environ. Sci. Technol., 45, 9866–9873, doi:10.1021/es2005545, 2011.

Duc, N. T., Crill, P., and Bastviken, D.: Implications of temperature and sediment characteristics on methane formation and oxidation in lake sediments, Biogeochemistry, 100, 185–196, doi:10.1007/s10533-010-9415-8, 2010.

Emery, W. J. and Thomson, R. E.: Data Analysis Methods in Physical Oceanography, Elsevier Science Limited, Amsterdam, the Netherlands, 2001.

Fang, X. and Stefan, H. G.: Dynamics of heat exchange between sediment and water in a lake, Water Resour. Res., 32, 1719–1727, 1996.

Fang, X. and Stefan, H. G.: Temperature variability in lake sediments, Water Resour. Res., 34, 717–729, doi:10.1029/96WR00274, 1998.

BGD
10, 18687–18722, 2013

Forster, P., Ramaswamy, V., Artaxo, P., Berntsen, T., Betts, R., Fahey, D. W., Haywood, J., Lean, J., Lowe, D. C., Myhre, G., Nganga, J., Prinn, R., Raga, G., Schulz, M., and Van Dorland, R.: Changes in Atmospheric Constituents and in Radiative Forcing, in: Climate Change, The Physical Science Basis, Contribution of Working Group I to the Fourth Assessment Report of the Intergovernmental Panel on Climate Change, edited by: Solomon, S., Qin, D., Manning, M., Chen, Z., Marquis, M., Averyt, K. B., Tignor, M., and Miller, H. L., Cambridge University Press, Cambridge, United Kingdom and New York, NY, USA, 2007.

Goodrich, J. P., Varner, R. K., Frolking, S., Duncan, B. N., and Crill, P. M.: High-frequency measurements of methane ebullition over a growing season at a temperate peatland site, Geophys. Res. Lett., 38, doi:10.1029/2011GL046915, 2011.

Hamblin, P. F. and Hollan, E.: On the gravitational seiches of Lake Constance and their generation, Schweiz. Z. Hydrol., 40, 119–154, doi:10.1007/BF02502376, 1978.

Hofmann, H., Lorke, A., and Peeters, F.: The relative importance of wind and ship waves in the littoral zone of a large lake, Limnol. Oceanogr., 53, 368, doi:10.4319/lo.2008.53.1.0368, 2008.

Hofmann, H., Federwisch, L., and Peeters, F.: Wave-induced release of methane: littoral zones as a source of methane in lakes, Limnol. Oceanogr., 55, 1990–2000, doi:10.4319/lo.2010.55.5.1990, 2010.

Jöhnk, K. D., Straile, D., and Ostendorp, W.: Water level variability and trends in Lake Constance in the light of the 1999 centennial flood, Limnologica-Ecology and Management of Inland Waters, 34, 15–21, doi:10.1016/S0075-9511(04)80017-3, 2004.

Johnson, B. D., Boudreau, B. P., Gardiner, B. S., and Maass, R.: Mechanical response of sediments to bubble growth, Mar. Geol., 187, 347–363, doi:10.1016/S0025-3227(02)00383-3, 2002.

Joyce, J. and Jewell, P. W.: Physical controls on methane ebullition from reservoirs and lakes, Environ. Eng. Geosci., 9, 167–178, doi:10.2113/9.2.167, 2003.

Kundu, P. K. and Cohen, I. M.: Fluid Mechanics, 4th edn., Elsevier Academic Press, Burlington, USA, 2008.

Leifer, I. and Patro, R. K.: The bubble mechanism for methane transport from the shallow sea bed to the surface: a review and sensitivity study, Cont. Shelf Res., 22, 2409–2428, doi:10.1016/S0278-4343(02)00065-1, 2002.

BGD
10, 18687–18722, 2013

Liikanen, A. and Martikainen, P. J.: Effect of ammonium and oxygen on methane and nitrous oxide fluxes across sediment–water interface in a eutrophic lake, Chemosphere, 52, 1287–1293, doi:10.1016/S0045-6535(03)00224-8, 2003.

Lorke, A., McGinnis, D. F., Maeck, A., and Fischer, H.: Effects of ship locking on sediment oxygen uptake in impounded rivers, Water Resour. Res., 48, WR012514, doi:10.1029/2012WR012483, 2012.

Maeck, A. and Lorke, A.: Ship-lock induced surges in an impounded river and their impact on subdaily flow velocity variation, River Res. Appl., doi:10.1002/rra.2648, 2013.

Maeck, A., DelSontro, T., McGinnis, D. F., Fischer, H., Flury, S., Schmidt, M., Fietzek, P., and Lorke, A.: Sediment trapping by dams creates methane emission hot spots, Environ. Sci. Technol., 47, 8130–8137, doi:10.1021/es4003907, 2013.

McGinnis, D., Greinert, J., Artemov, Y., Beaubien, S., and Wüest, A.: Fate of rising methane bubbles in stratified waters: how much methane reaches the atmosphere?, J. Geophys. Res.-Oceans, 111, C09007, 8130–8137, doi:10.1029/2005JC003183, 2006.

Scandella, B. P., Varadharajan, C., Hemond, H. F., Ruppel, C. and Juanes, R.: A conduit dilation model of methane venting from lake sediments, Geophys. Res. Lett., 38, L06408, doi:10.1029/2011GL046768, 2011.

Schöl, A.: Die Saar – Auswirkungen der Stauregelung auf den Sauerstoffhaushalt in einem abflussarmen Mittelgebirgsfluss, in: Staugeregelte Flüsse in Deutschland, edited by: Kinzelbach, F. G., Ragnar, Stuttgart, Germany, 2006.

Segers, R.: Methane production and methane consumption: a review of processes underlying wetland methane fluxes, Biogeochemistry, 41, 23–51, doi:10.1023/A:1005929032764, 1998.

Sobek, S., DelSontro, T., Wongfun, N., and Wehrli, B.: Extreme organic carbon burial fuels intense methane bubbling in a temperate reservoir, Geophys. Res. Lett., 39, L01401, doi:10.1029/2011GL050144, 2012.

UNESCO/IHA: GHG Measurement Guidelines for Freshwater Reservoirs, edited by: Goldenfum, J. A., UNESCO, IHA, 2010.

USACE: Hydaulic design – surges in canals – change 1, in: Engineering and Design, US Army Corps of Engineering, Washington, DC, USA, 1–15, 1949.

Varadharajan, C. and Hemond, H. F.: Time-series analysis of high-resolution ebullition fluxes from a stratified, freshwater lake, J. Geophys. Res.-Biogeo., 117, G02004, doi:10.1029/2011JG001866, 2012.

BGD
10, 18687–18722, 2013

Venkiteswaran, J. J., Schiff, S. L., St. Louis, V. L., Matthews, C. J., Boudreau, N. M., Joyce, E. M., Beaty, K. G., and Bodaly, R. A.: Processes affecting greenhouse gas production in experimental boreal reservoirs, Global Biogeochem. Cy., 27, 1–11, doi:10.1002/gbc.20046, 2013.

Wilcox, D. A., Thompson, T. A., Booth, R. K., and Nicholas, J.: Lake-level variability and water availability in the Great Lakes, US Geological Survey, 2007.

Zohary, T. and Ostrovsky, I.: Do water level fluctuations matter?, Inland Waters, 1, 47–59, 2011.

BGD
10, 18687–18722, 2013

Table 1. Monthly mean ± std. and overall mean ± std. concentration of CH_4 in captured bubbles of the three automated bubble traps (ABTs) during the entire sampling period.

	Nov [% CH_4]	Dec [% CH_4]	Jan [% CH_4]	Feb [% CH_4]	Mar [% CH_4]	Mean ± std. per ABT [% CH_4]
ABT-1	89.8	81.1	48.6	71.1	89.5	76.0 ± 17.1
ABT-2	89.2	80.9	76.6	78.0	88.5	82.6 ± 5.9
ABT-3	89.5	84.2	72.8	75.0	92.1	82.7 ± 8.6
Monthly mean ± std	89.5 ± 0.3	82.1 ± 1.8	66.0 ± 15.2	74.7 ± 3.5	90.0 ± 1.9	80.5 ± 10.2

BGD
10, 18687–18722, 2013

Table 2. Results of the multiple logistic regression analysis of ebullition rates observed at the automated bubble traps 1 to 3 (ABT) and physical forcing mechanisms. Percentages indicate the contribution of each factor to the logistic model.

	ABT-1	ABT-2	ABT-3
Atmospheric pressure change	11.3 % (+)	2.9 % (+)	5.8 % (+)
Low frequent hydrostatic pressure change	10.6 % (+)	7.3 % (+)	7.3 % (+)
High frequency pressure fluctuations	17.8 % (+)	6.9 % (+)	17.2 % (–)
Ebullition of the previous 24 h	50.2 % (–)	79.8 % (–)	61.6 % (–)
Discharge	10.2 % (–)	3.1 % (–)	8.0 % (–)

BGD
10, 18687–18722, 2013

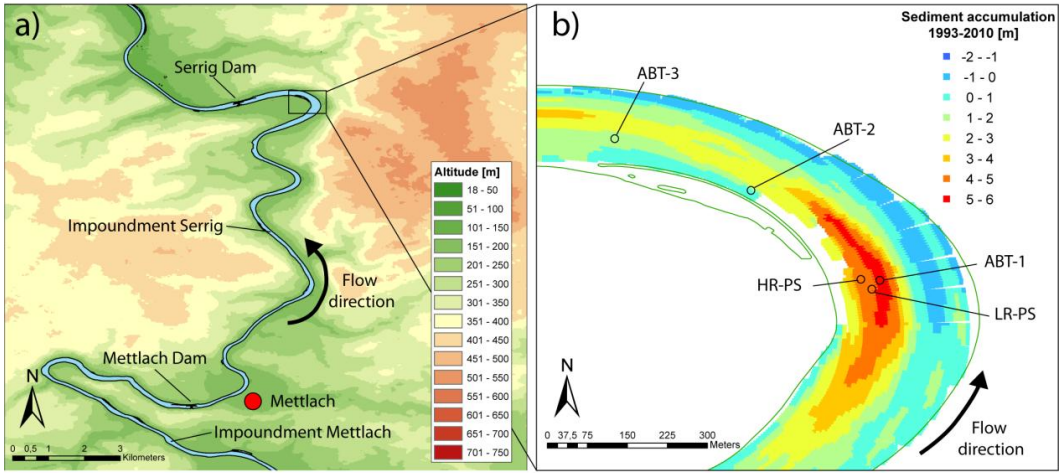

Fig. 1. Location of the sampling sites. **(a)** Topographic map of the Serrig impoundment (49.576° N, 6.600° E), which is enclosed by the upper dam in Mettlach and the lower dam in Serrig. The sampling sites are located ~ 1 to 2 km upstream of Serrig dam in the inner bending of the river meander. **(b)** Map of the sampling sites showing sediment accumulation within the Serrig impoundment (Maeck et al., 2013). The positions of deployment sites for three automatic bubble traps (ABT 1 to 3), the high-resolution pressure sensors (HR-PS) and the low-resolution pressure sensor (LR-PS) are indicated.

BGD
10, 18687–18722, 2013

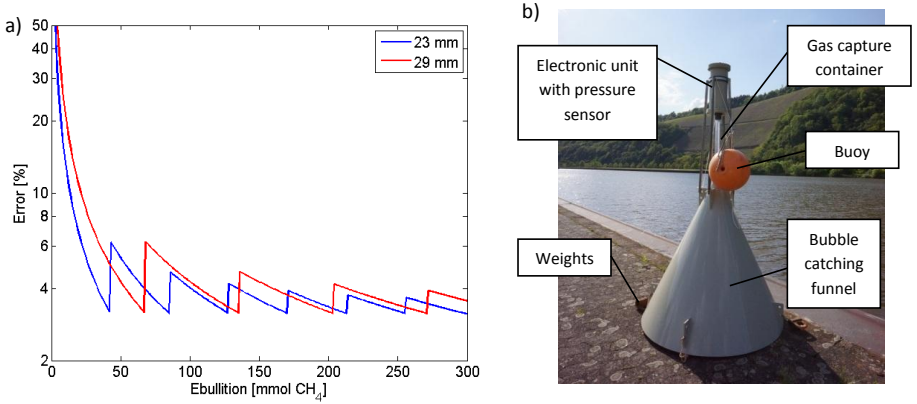

Fig. 2. (a) Error in the volume determination in relation to the captured gas for two different diameters of the gas capture container (23 and 29 mm). The saw-like steps in the curve result from venting of the system and the start of a new filling cycle. Since for every cycle two additional differential pressure sensor readings are necessary, error increases temporarily due to flushing. **(b)** Automated bubble trap device. The instrument operates submerged and catches rising bubbles. The captured gas is stored in the cylindrical gas capture container and the fill height of the container is measured via differential pressure with the electronic unit.

BGD
10, 18687–18722, 2013

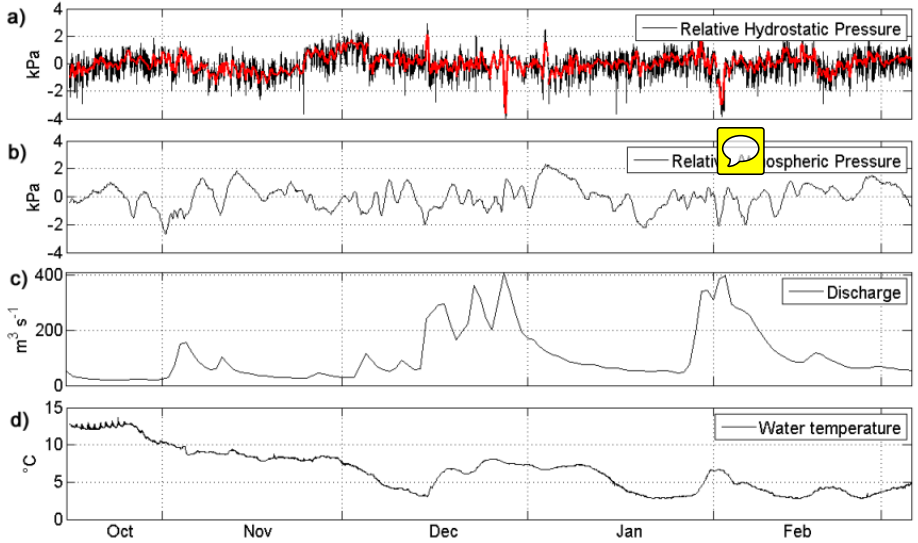

Fig. 3. (a) Relative hydrostatic (original data in black, low-frequency filtered in red), **(b)** atmospheric pressure, **(c)** discharge and **(d)** water temperature between 16 October 2012 and 6 March 2013.

BGD
10, 18687–18722, 2013

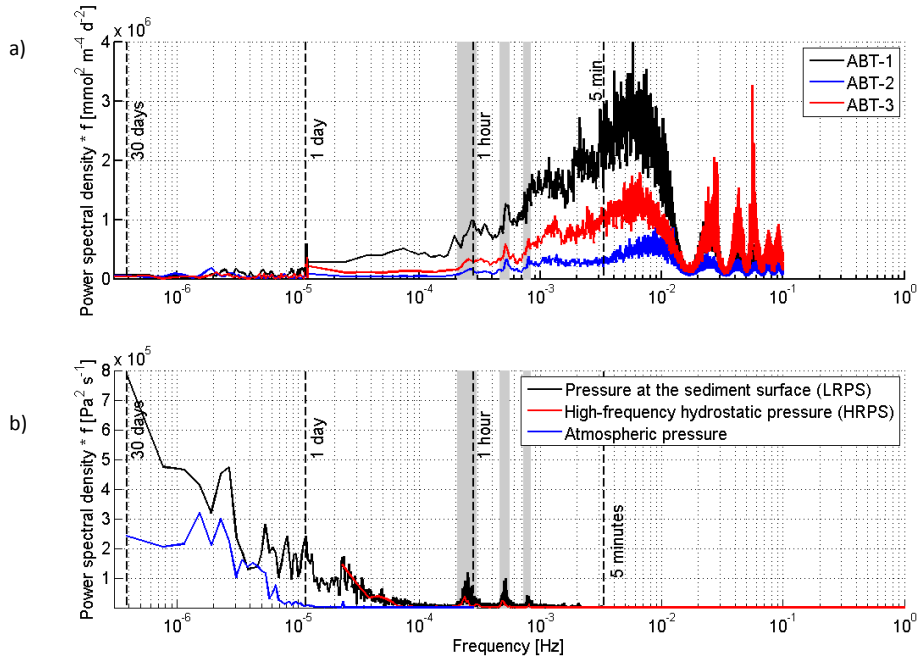

Fig. 4. Variance preserving power spectra of ebullition rates **(a)** and hydrostatic (LR-PS and HR-PS) and atmospheric pressure in **(b)**. Peaks at 15 min, 30 min and 1 h are marked in grey and caused by ship-lock induced surges.

BGD
10, 18687–18722, 2013

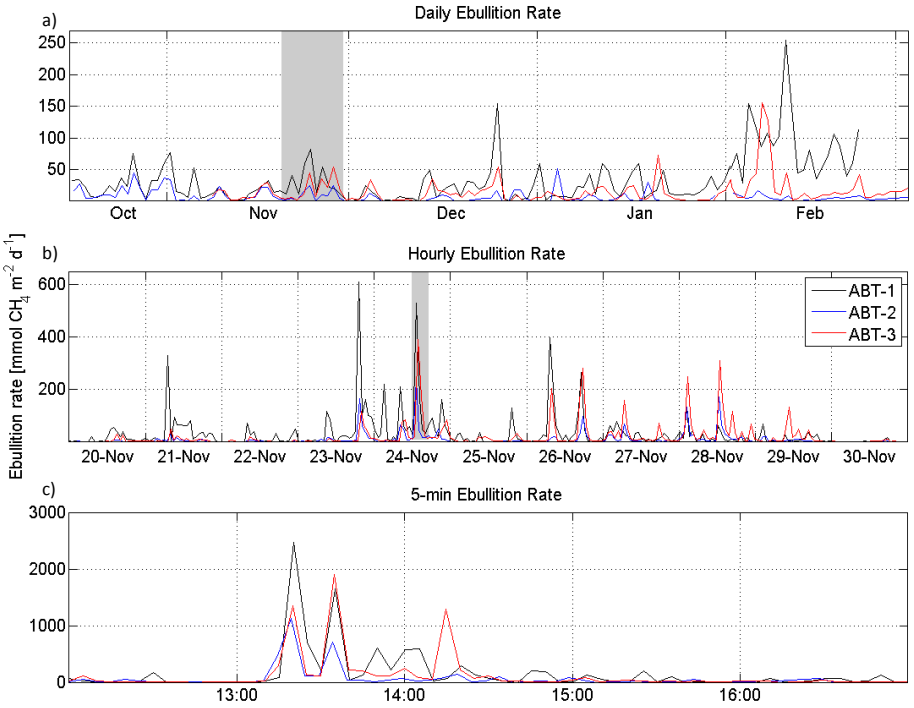

Fig. 5. Temporal variability of ebullition rates observed using the three automated bubble traps (ABTs) at different time scales: **(a)** daily mean ebullition rates for the entire sampling period. **(b)** Hourly mean and **(c)** 5 min mean ebullition rates for selected time periods indicated by the grey bars in **(a)** and **(b)**.

BGD
10, 18687–18722, 2013

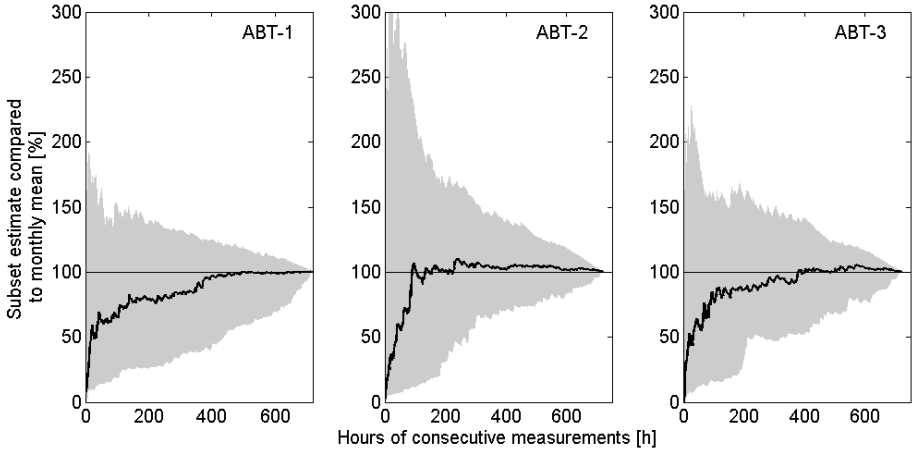

Fig. 6. Mean ebullition rates averaged over subsets of varying length representing consecutive measurement periods normalizhed by the mean ebullition rate observed over a 30 day period centered around the respective subset for the automated bubble traps (ABT 1–3) (left to right). The black line shows the median of all subsets and the grey area denotes the 10 and 90-percentiles.

BGD
10, 18687–18722, 2013

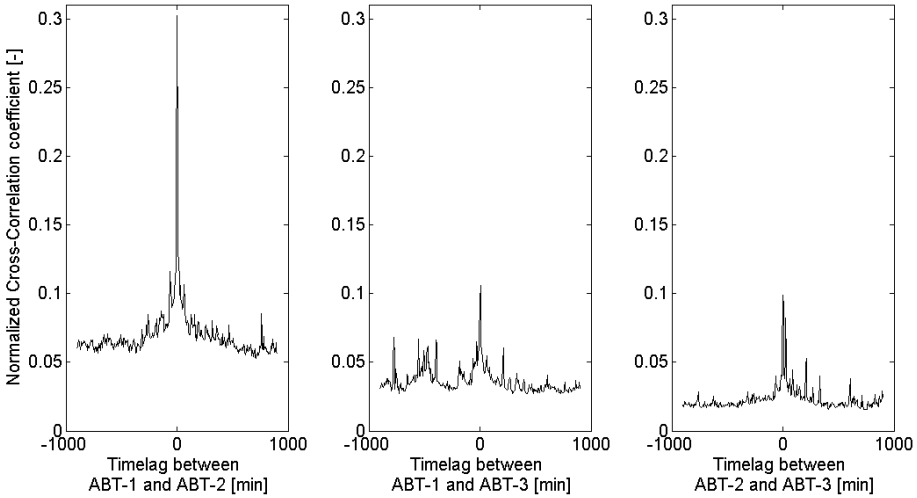

Fig. 7. Cross-correlation coefficients of the 5 min ebullition rates vs. the time lag of the three ABTs against each other. Peaks at zero lag indicate that both signals are synchronized.

BGD
10, 18687–18722, 2013

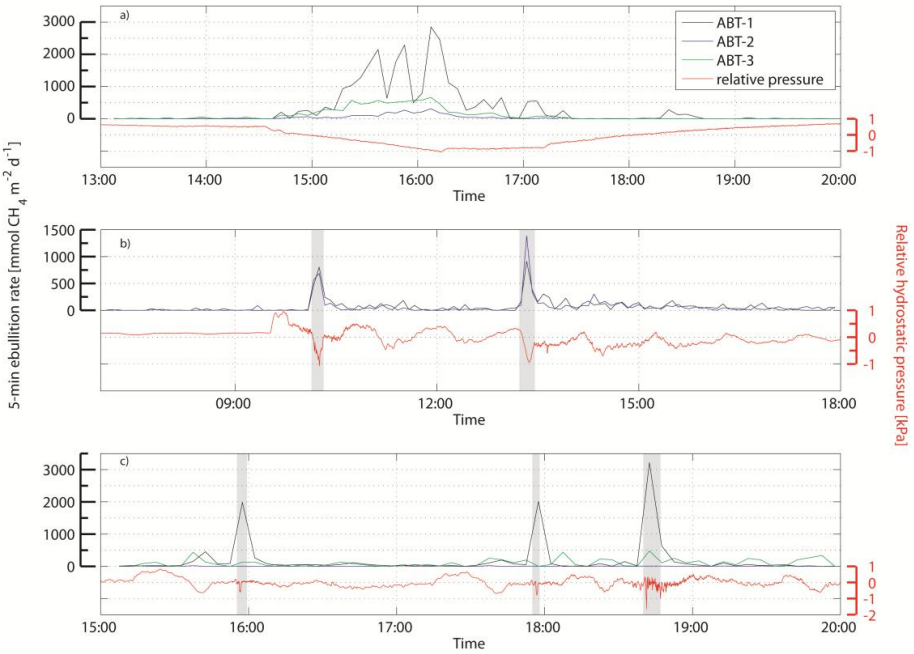

Fig. 8. Timeseries of 5 min ebullition rates and hydrostatic pressure changes. Panel **(a)** shows bubble release during sinking water level within a high-discharge period (25 December 2012). Panel **(b)** shows the relationship between positive and negative (grey shaded) surges and the ebullition rates (31 October 2012) while panel **(c)** highlights ebullition during corresponding ship-passages (grey shaded) (18 Febuary 2013).

BGD
10, 18687–18722, 2013

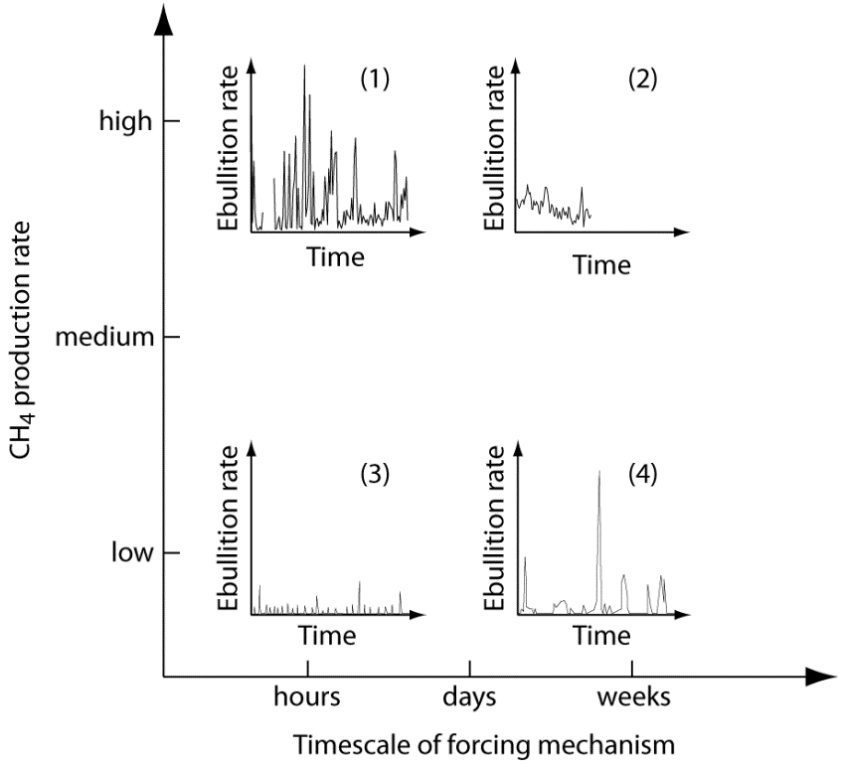

Fig. 9. Conceptual framework for characterizing temporal variability of ebullition in aquatic systems differing in CH_4 production rates, estimated by using the sedimentation rate as a proxy, and forcing time scales for ebullition. All examples show ebullition rates (6 h average) over a period of 4 weeks, except for (2) which refers to a period of 2 weeks. Example (1) shows the measured data from this study (Saar, ABT-1, January 2013), example (2) shows measured data from the River Main, Germany, (Krotzenburg Dam, September 2012) and example (4) shows measurements from the Upper Mystic Lake (25 m site, October) taken from Varadharajan et al. (2012). Example (3) is a conceptual example.

BGD
10, 18687–18722, 2013